NANO LETTERS

2006
Vol. 6, No. 4
599−604

Influence of Nanowire Density on the Shape and Optical Properties of Ternary InGaAs Nanowires

Yong Kim,[†,‡] Hannah J. Joyce,[†] Qiang Gao,[†] H. Hoe Tan,[†] Chennupati Jagadish,*[,†] Mohanchand Paladugu,[§] Jin Zou,[§] and Alexandra A. Suvorova[||]

Department of Electronic Materials Engineering, Research School of Physical Sciences and Engineering, The Australian National University, Canberra, ACT 0200, Australia, Department of Physics, Dong-A University, Hadan-2-dong, Sahagu, Busan 604-714, Korea, School of Engineering and Centre for Microscopy and Microanalysis, The University of Queensland, Brisbane, QLD 4072, Australia, and Centre for Microscopy and Microanalysis, The University of Western Australia, Crawley, WA 6009, Australia

Received November 6, 2005; Revised Manuscript Received January 23, 2006

ABSTRACT

We have synthesized ternary InGaAs nanowires on (111)B GaAs surfaces by metal−organic chemical vapor deposition. Au colloidal nanoparticles were employed to catalyze nanowire growth. We observed the strong influence of nanowire density on nanowire height, tapering, and base shape specific to the nanowires with high In composition. This dependency was attributed to the large difference of diffusion length on (111)B surfaces between In and Ga reaction species, with In being the more mobile species. Energy dispersive X-ray spectroscopy analysis together with high-resolution electron microscopy study of individual InGaAs nanowires shows large In/Ga compositional variation along the nanowire supporting the present diffusion model. Photoluminescence spectra exhibit a red shift with decreasing nanowire density due to the higher degree of In incorporation in more sparsely distributed InGaAs nanowires.

The anisotropic growth of silicon whiskers via the vapor−liquid−solid (VLS) growth mechanism was discovered by Wagner and Ellis.[1] According to this mechanism, a small Au particle on the semiconductor surface forms a eutectic liquid alloy with the host material at growth temperature. The liquid droplet is an ideal sink for reaction species supplied from the surrounding vapor and is readily supersaturated with reaction species. The precipitation of reaction species at the solid/liquid interface leads to highly anisotropic whisker growth. The kinetics of the VLS growth mode was extensively investigated in the 1970s. Specifically the correlation between silicon whisker height and the diameter of the Au liquid droplet was explained in terms of the Gibbs−Thomson effect.[2] Nanowires, scaled down in dimensions from these micrometer-sized whiskers, have gained much interest due to their potential in nano-optoelectronics applications.[3]

Recently, axial and radial heterostructure nanowires[4] have been proposed as promising nano building blocks for future optoelectronic devices, with superior properties to conventional layered heterostructures. Nanowire lasers,[5,6] resonant tunneling diodes,[7] and single electron tunneling diodes[8] have been demonstrated. In addition, it is predicted that free standing III−V nanowires with high crystallographic perfection can be grown even on highly lattice-mismatched substrates due to radial expansion/contraction of the lattice constant. Indeed, successful fabrication of III−V nanowires on Si/Ge substrates has been demonstrated.[9,10] Despite the large thermal, chemical, and structural mismatch between these highly dissimilar materials, high crystallographic and optical qualities were reported.[9,10] The VLS growth mechanism has been questioned specifically for III−V nanowire growth. InAs nanowires have been grown by pure Au particle assistance only in the temperature range where the particle forms a solid alloy with supplied In.[11] A vapor−solid−solid (VSS) mechanism rather than VLS mechanism has been proposed.[12]

These recent successes particularly in III−V nanowires have been largely limited to binary nanowires. However, ternary nanowires are obviously required for fabricating complex radial/axial heterostructures. Some optical properties of ternary AlGaAs nanowires have been reported.[13] Further systematic studies, with emphasis on the uniform growth of

* Corresponding author. E-mail: chennupati.jagadish@anu.edu.au.
[†] The Australian National University.
[‡] Dong-A University.
[§] The University of Queensland.
[||] The University of Western Australia.

10.1021/nl052189o CCC: $33.50
Published on Web 02/21/2006

ternary nanowires with device-accessible structural and optical properties, are important. In this paper, we focus on ternary InGaAs nanowires due to the paramount importance of this material system for applications in long wavelength optical transmission and integrated photonics. We investigate the shape/height control of InGaAs nanowires grown by metal−organic chemical vapor deposition (MOCVD), in conjunction with their optical properties.

Undoped GaAs (111)B substrates were functionalized by dipping in 0.1% poly-L-lysine (PLL) solution for 1 min. After being rinsed with deionized (DI) water, the substrates were blown dry with N_2 gas. A 100 μL drop of commercially available Au colloid liquid containing 30 ± 3 nm diameter Au nanoparticles diluted to the density of 1×10^{11} particles/mL was dispersed on the substrate surface and rinsed off with DI water after 30 s. This method is similar to those reported previously.[14,15] The PLL layer acts as a positively charged polyelectrolyte which attracts negatively charged Au nanoparticles and immobilizes them on the substrate surface. PLL treatment has been used for the immobilization of nanoparticles to create standard samples for atomic force microscope calibration.[16]

InGaAs nanowires were grown by horizontal flow MOCVD at a pressure of 100 mbar. The total flow rate of H_2 carrier gas in the reactor cell was 15 standard L/min. Prior to nanowire formation, the substrate was annealed in situ at 600 °C under AsH_3 ambient for 10 min to desorb surface contaminants and form the eutectic alloy between Au nanoparticles and Ga from the substrate. After cooling down to the desired growth temperature, group III source gases are switched on to initiate nanowire growth. The molar flow rates of trimethylgallium (TMG) and AsH_3 were 1.2×10^{-5} and 5.4×10^{-4} mol/min, respectively. Trimethylindium (TMI) molar flow rates between 0 and 3.5×10^{-6} mol/min were selected to yield vapor In compositions (x_v) of 0, 0.11, 0.19, and 0.23. Vapor In mole fractions during growth were precisely determined by a real time acoustic sensor. GaAs nanowires were grown in the absence of TMI for reference. Growth temperature and time were 450 °C and 30 min, respectively, for all samples. This growth temperature was the optimized temperature for GaAs nanowire growth determined from previous experiments. Since the Au colloidal solution was applied as a droplet, a circular pattern of nanowires on the substrate was obtained after the growth. The colors within this circle change with viewing angle due to diffraction effects. A nonuniform nanowire distribution within the circle was apparent even by visual inspection. This was further confirmed by optical microscopy. In general, nanowire density is the highest in the circle center and decreases gradually toward the edge of the circle.

Field emission scanning electron microscope (FE-SEM) images of regions between the circle center and edge were obtained for each sample. Nanowire density and height distribution were measured within each imaged region. Transmission electron microscopy (TEM) specimens were prepared in the following manner. The nanowire sample was put into a container with ethanol. The sample in the container was sonicated for 20 min in order to cut the nanowires from their underlying substrate. These TEM specimens were then dispersed onto a holey carbon film. TEM experiments were carried out in a FEI tacnai F30 and a JEOL 3000F TEM operating at 300 kV. Bright-field image and high-resolution electron microscopy (HREM) were employed to study the nanostructure and nanomorphology of these nanowires. The compositional variations within nanowires were studied using energy dispersive X-ray spectroscopy (EDS). This work was carried out using a JEOL 3000F field emission gun TEM equipped with an Oxford Instruments INCA 200 EDS system and STEM. For each nanowire, the EDS spectra were taken at three different locations (close to Au catalyst, in the middle and at the base end of a nanowire). The In/Ga ratio in the nanowires was evaluated by comparing In Lα and Ga Kα X-ray peaks using the ISIS software.

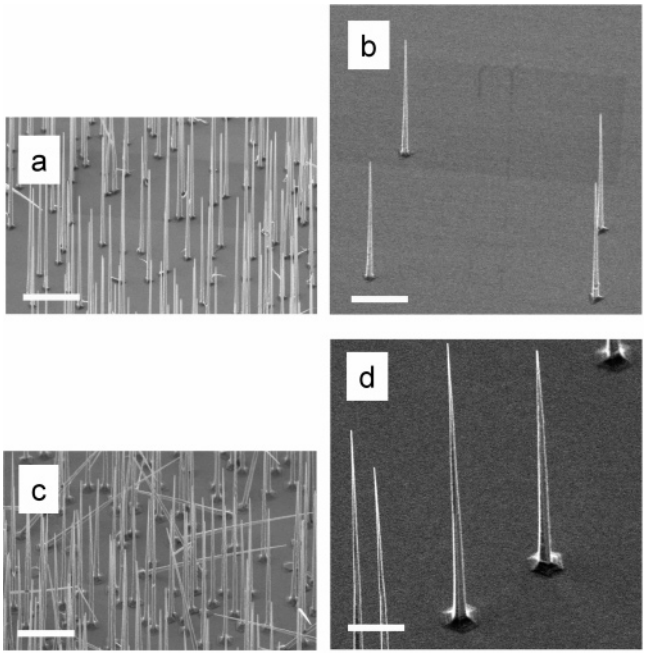

Figure 1. 45° tilt FESEM images of InGaAs nanowires. (a, b) FESEM images of InGaAs nanowires with x_v of 0.11. (c, d) FESEM images of InGaAs nanowires with x_v of 0.19. The nanowires in parts a and c have almost equal available diffusion areas of approximately 1.4 μm^2. The nanowires in parts b and d have available diffusion areas of approximately 67 μm^2. Scale bars are 2 μm.

Figure 1 shows FE-SEM images taken with the substrate tilted 45° from the e-beam. Most nanowires grow perpendicular to the substrate surface in the ⟨111⟩B direction, which is the energetically favorable direction. However, as observed in Figure 1c, there are some inclined nanowires presumably having different growth directions to ⟨111⟩. These inclined nanowires are generally longer and were excluded from the present statistical investigation of nanowire density and height. Parts a and b of Figure 1 show InGaAs nanowires grown with an x_v of 0.11. In Figure 1a, the nanowire density is 0.73 μm^{-2}, whereas the density in Figure 1b is 0.015 μm^{-2}. Parts c and d of Figure 1 are images of InGaAs nanowires grown at a higher x_v of 0.19. The densities of parts c and d of Figure 1 are 0.70 and 0.018 μm^{-2}, respectively. For the nanowires with lower In composition, as shown in parts a and b of Figure 1, there is no significant density dependency

of nanowire height. The same trend was observed for GaAs nanowires. In contrast, the nanowires grown at the higher x_v exhibit drastic height enhancement in the low-density region: the average height in Figure 1c was 5.8 ± 0.1 μm, whereas average height in Figure 1d was 13 ± 0.8 μm. Thus the height enhancement is more than a factor of 2. We observe similar height enhancement for InGaAs nanowires with x_v of 0.23.

One-dimensional nanowire growth in MOCVD has been modeled to describe the temperature-dependent variation of nanowire height.[17] This model considers two major contributions of reaction species to axial nanowire growth. First is the species directly impinging on the Au nanoparticle residing on the top of nanowire. Second is the species that arrive at the nanowire side walls and subsequently diffuse along the side walls toward Au nanoparticle. The model has been extended to include a third contribution[18] arising from the species that initially arrive at the (111)B substrate surface, travel on the surface and finally diffuse toward the Au nanoparticle. This third contribution is important for explaining our result. In the case of ternary InGaAs nanowires, the diffusion of both In and Ga species must be considered. We believe the diffusion length, which is the average migration distance of reaction species before incorporation, of In species on the (111)B substrate surface is much larger than that of Ga species. The concept of available diffusion area, defined as the inverse of nanowire density, will give much physical insight since its square root value roughly matches to available diffusion distance and thereby gives the information about the diffusion lengths of the two species.

Parts a−d of Figure 2 show FE-SEM images of representative nanowires grown with x_v between 0 and 0.23. Their available diffusion areas are larger than 40 μm^2. As discussed later, such a large available diffusion area means these nanowires are effectively isolated and subject to minimal interference from neighboring nanowires during growth. The nanowires of parts c and d of Figure 2, grown at high x_v, are significantly taller than those of parts a and b of Figure 2, grown at lower x_v. This provides evidence of height enhancement specific to high In composition nanowires at low nanowire density. The heights of GaAs nanowires and InGaAs nanowires with an x_v of 0.11 (Figure 2a,b) appear the same. However, more tapering is observed in Figure 2b compared to the GaAs nanowire of Figure 2a, indicating the incorporation of In species near the bottom of nanowire following diffusion from the substrate surface. Together with systematic enhancement of tapering with increasing In composition, the base shape change is also interesting. The triangular base of GaAs nanowires in Figure 2a, develops to a hexagonal base shape in parts c and d of Figure 2 accompanied by widening of the base. The detailed mechanism for such a base-shape change could be substantiated by extensive TEM experiments focused on the interface between nanowire and substrate. Parts e−i of Figure 2 show the evolution of the base for InGaAs nanowires with x_v of 0.23 with increasing available diffusion area. The elbow at the intersection between a nanowire and the substrate has a higher growth rate with increasing available diffusion area

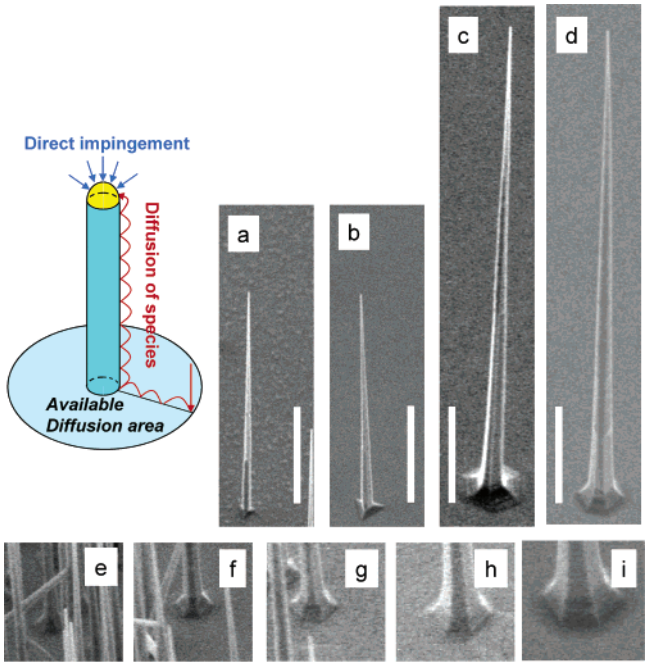

Figure 2. (a−d) 45° tilt FESEM images of representative InGaAs nanowires grown with different x_v of (a) 0 (i.e. GaAs nanowires), (b) 0.11, (c) 0.19, and (d) 0.23. All images were taken from the regions with the available diffusion area larger than 40 μm^2. Therefore, these nanowires are effectively isolated from the influence of neighboring nanowires during growth. Scale bars are 2 μm. (e−i) 45° tilt FESEM images showing the base shape evolution with increasing available diffusion area for InGaAs nanowires with x_v of 0.23. Imaging area is 1.5 × 1.5 μm^2. The available diffusion areas are (e) 0.65, (f) 1.58, (g) 3.70, (h) 20.8, and (i) 33.3 μm^2, respectively. A schematic picture illustrating the concept of available diffusion area is also included.

and develops into the base.[19] This confirms that base widening is strongly correlated with the surface diffusion of reaction species. In addition, the hexagonal base shape is retained even for nanowires with very low available diffusion area as shown in Figure 2e. The shape-determining factor is therefore not the nanowire density or the available diffusion length but the In composition. In the case of GaAs nanowires, there is no apparent density-dependent widening of the base across all observation areas.

Figure 3a shows the nanowire height variation as a function of available diffusion area. Regardless of x_v, nanowire height increases significantly with available diffusion area provided available diffusion area is less than a few square micrometers. At higher available diffusion area, GaAs nanowires and InGaAs nanowires with x_v of 0.11 exhibit height saturation. In contrast, the heights of InGaAs nanowires with higher x_v continue to increase and exhibit height saturation at a larger available diffusion area of approximately 30-40 μm^2. We speculate the initial increase is related to Ga diffusion length. When available diffusion area exceeds Ga diffusion length, the heights of GaAs or InGaAs nanowires with low x_v, will saturate. Therefore, the Ga diffusion length is less than 2 μm on the (111)B GaAs surface. It is well-known that In species have a larger diffusion length than Ga species. This difference has led to the In content increase near the mask edges during the

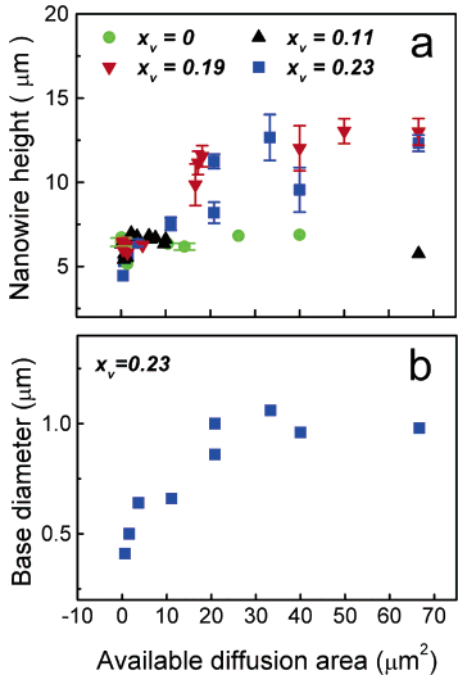

Figure 3. (a) Nanowire height vs available diffusion area for InGaAs nanowires with x_v of 0, 0.11, 0.19, and 0.23. (b) Base diameter vs available diffusion area for InGaAs nanowires with x_v of 0.23.

selective area epitaxy of InGaAs by low-pressure MOCVD growth.[20,21] Recently this difference has been utilized for emission wavelength tuning of InGaAs quantum dots during selective area epitaxy.[22] From the height saturation behavior of InGaAs nanowires with higher x_v, the In diffusion length on the surface is estimated at approximately 6 μm (i.e., 5.5−6.3 μm from the square root value of the available diffusion area at the height saturation point). It is noteworthy that the diffusion length we discuss is that on (111)B GaAs surfaces. One may add nanowire height to the diffusion lengths on (111)B surface for an estimate of total diffusion length. However, in this report, discussion is limited to the diffusion length difference on (111)B surfaces because this gives more insight into tapering and base-shape change. Figure 3b shows the base diameter variation of InGaAs nanowires with an x_v of 0.23. The base diameter was fairly uniform within the scanning area though height showed some statistical fluctuation. The base width shows a similar trend to nanowire height with saturation at an available diffusion area of approximately 30-40 μm^2. This result confirms again that the main reason for height enhancement is the incorporation of species diffused from substrate surface. A recent investigation of the surface diffusion of In species on InAs (111)B substrates in chemical beam epitaxy of InAs nanowires has shown similar saturation behavior in nanowire height but at an available diffusion area of approximately 1 μm^2.[23] This is an order of magnitude smaller than the present result.

Figure 4a shows a HREM image of a nanowire with the catalyst on top of the wire. The zinc blende crystal structure together with some stacking faults is clearly seen in the nanowire. HREM also confirmed the growth direction being ⟨111⟩. At present, we cannot draw any conclusion whether the nanowire shown in Figure 4a is grown by VLS or VSS mechanisms. However, because our report is primarily focused on the influence of nanowire density on nanowire height and base shape, the growth mechanism does not affect our conclusion. Figure 4b shows the low-resolution TEM image of a nanowire. Markers indicate the EDS measurement positions. As observed in the EDS spectra of Figure 4c, there is remarkable In/Ga variation along the InGaAs nanowire. The diffusion model we introduced would mean the gradual variation in chemical composition along the nanowires, with greater In corporation toward the nanowire base. The EDS results clearly support the model. The In/Ga compositional ratio near the tip of the nanowire was 0.27 (x_s = 0.21), and the value is very close to the vapor In composition, x_v of 0.19. In/Ga compositional variations were measured from several InGaAs nanowires with the same x_v of 0.19. We observed similar strong In/Ga compositional variations along these nanowires.

Low-temperature photoluminescence (PL) measurements were performed at 10 K to characterize the emission energy shift of InGaAs nanowires depending on nanowire density. Nanowires were excited by a diode-pumped solid-state frequency-doubled green laser at 532 nm. PL was dispersed by a 0.5 m monochromator and detected by a thermoelectrically cooled InGaAs photodetector. Figure 5 shows PL spectra of InGaAs nanowires with an x_v of 0.19 measured at the different positions of the circular pattern. PL intensity is primarily related to nanowire density, with PL peak intensity gradually decreasing as the laser spot is traced from regions of high to low nanowire density. This confirms that the PL in Figure 4 arises from nanowires. The broadness of PL spectra is presumably due to a spread in the chemical composition along nanowires, as observed in the EDS analysis of Figure 4c.

PL spectra consist of at least two peaks with different origins. As observed in Figure 4b, the higher energy PL peak undergoes a red shift together with the decrease in PL intensity, the decrease in nanowire density, and the consequent increase in available diffusion area. Since higher In composition is generally associated with a red shift in PL, the results indicate that average In composition increases with available diffusion area. This is in good agreement with our FE-SEM observations. The lower energy PL peak intensity decreases together with the decrease of high energy PL peak intensity. However, a PL shift is not apparent in this case. Thus, we speculate this PL peak is related to defects presumably occurring near the base of nanowires due to large lattice mismatch between the InGaAs nanowires and GaAs substrate. This is plausible because high In composition near the base of nanowires was observed (Figure 4b).

In summary, we have synthesized InGaAs nanowires by MOCVD. We have observed the strong influence of nanowire density on nanowire height and base shape. This dependency is attributed to the large difference of diffusion lengths between In and Ga species on the (111)B GaAs substrate, which determines the degree of In and Ga incorporation into nanowires. The estimated Ga diffusion length is less than 2 μm while In diffusion length is estimated

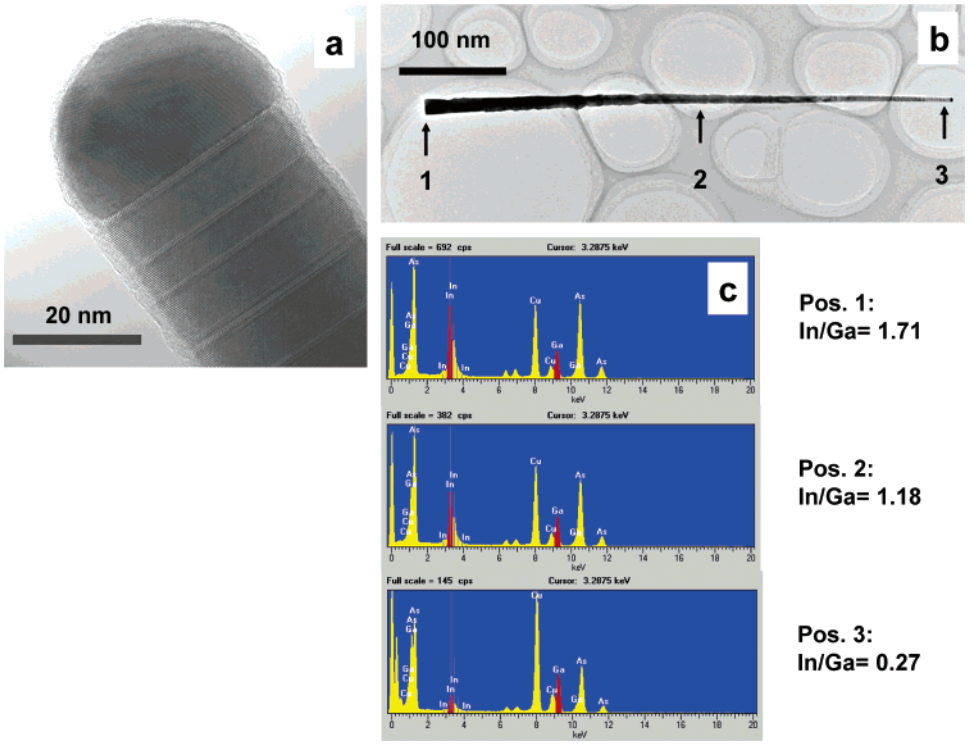

Figure 4. (a) HREM image of a nanowire ($x_v = 0.19$) with the Au catalyst on the top of the nanowire. (b) TEM image of InGaAs nanowire on a holey carbon grid. Markers indicate detection positions for EDS measurements. (c) EDS from various detection positions. Determined In/Ga ratios are also displayed.

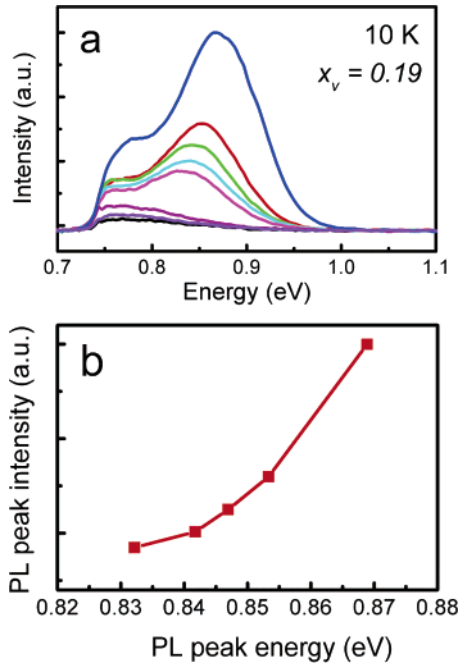

Figure 5. (a) PL spectra of InGaAs nanowires with x_v of 0.19 measured at 10 K. The spectra are taken from the different regions having different nanowire densities. PL intensity is primarily related to nanowire density. That is, higher intensity indicates higher density as confirmed by visual or optical microscope observations. (b) PL peak intensity as a function of peak energy.

at approximately 6 μm. The EDS analysis together with HREM study of individual InGaAs nanowires shows large In/Ga compositional variation along the nanowires supporting the present diffusion model. Increased In incorporation into nanowires with decreasing nanowire density leads to a red shift in PL peak. These results highlight the difficulty in controlling the composition and uniformity of ternary InGaAs nanowires during MOCVD growth, particularly for nanowires with higher In composition. Similar phenomena would be observed in other ternary nanowire systems with large differences in the diffusion lengths of constituent group III reaction species. Nevertheless, uniform and reliable ternary nanowire synthesis for photonic device fabrication could still be achieved by precise control of inter-nanowire distance.

Acknowledgment. We thank the Australian Research Council for the financial support. Y.K. thanks Dong-A University for financial support.

References

(1) Wagner, R. S.; Ellis.W. C. *Appl. Phys. Lett.* **1964**, *4*, 89.
(2) Givargizov, E. I. *J. Cryst. Growth* **1975**, *31*, 20.
(3) Hiruma, K.; Yazawa, M.; Haraguchi, K.; Ogawa, K.; Katsuyama, T.; Koguchi, M.; Kakibayashi, H. *J. Appl. Phys.* **1993**, *74*, 3162.
(4) Lieber, C. M. *MRS Bull.* **2003**, *28*, 486.
(5) Duan, X.; Huang, Y.; Agarwal, R.; Lieber, C. M. *Nature* **2003**, *421*, 241.
(6) Huang, M. H.; Mao, S.; Feick, H.; Yan, H.; Wu, Y.; Kind, H.; Weber, E.; Russo, R.; Yang, P. *Science* **2001**, *292*, 1897.
(7) Björk, M. T.; Ohlsson, B. J.; Thelander, C.; Persson, A. I.; Deppert, K.; Wallenberg, L. R.; Samuelson, L. *Appl. Phys. Lett.* **2002**, *81*, 4458.
(8) Thelander, C.; Nilsson, H. A.; Jensen, L. E.; Samuelson, L. *Nano Lett.* **2005**, *5*, 635.
(9) Mårtensson, T.; Svensson, C. P.T.; Wacaser, B. A., Larsson, M. W.; Seifert, W.; Deppert, K.; Gustafsson, A.; Wallenberg, L. R.; Samuelson, L. *Nano Lett.* **2004**, *4*, 1987.
(10) Bakkers, E. P. A. M.; van Dam, J. A.; De Franceschi, S.; Kouwenhoven, L. P.; Kaiser, M.; Verheijen, M.; Wondergem, H.; van der Sluis, P. *Nat. Mater.* **2004**, *3*, 769.

(11) Dick, K. A.; Deppert, K.; Mårtensson, T.; Mandl, B.; Samuelson, L.; Seifert, W. *Nano Lett.* **2005**, *5*, 761.
(12) Persson, A. I.; Larsson, M. W.; Stenström, S.; Ohlsson, B. J.; Samuelson, L.; Wallenberg, L. R. *Nat. Mater.* **2004**, *3*, 677.
(13) Wu, Z. H.; Sun, M.; Mei, X. Y.; Ruda, H. E. *Appl. Phys. Lett.* **2004**, *26*, 657.
(14) Cui, Y.; Lauhon, L. J.; Gudiksen, M. S.; Wang, J.; Lieber, C. M. *Appl. Phys. Lett.* **2001**, *78*, 2214.
(15) Hochbaum, A. I.; Fan, R.; He, R.; Yang, P. *Nano Lett.* **200***5*, *5*, 457.
(16) Vesenka, J.; Manne, S.; Giberson, R.; Marsh, T.; Henderson, E. *Biophys. J.* **1993**, *65*, 1.
(17) Seifert, W.; Borgström, M.; Deppert, K.; Dick; K. A.; Johansson, J.; Larsson, M. W.; Mårtensson, T.; Sköld, N.; Sevensson, C. P.; Wacaser, B. A.; Wallenberg, L. R.; Samuelson, L. *J. Cryst. Growth* **2004**, *272*, 211.
(18) Johansson, J.; Svensson, C. P. T.; Mårtensson, T.; Samuelson, L.; Seifert, W. *J. Phys. Chem. B* **2005**, *109*, 13567.
(19) Persson, A. I.; Ohlsson, B. J.; Jeppesen, S.; Samuelson, L. *J. Cryst. Growth* **2004**, *272*, 167.
(20) Zimmermann, G.; Ougazzaden, A.; Gloukhian, A.; Rao, E. V. K.; Delprat, D.; Ramdane, A; Mircea, A. *J.* Cryst. *Growth* **1997**, *170*, 645.
(21) Ida, M.; Shigekawa, N.; Furuta, T.; Ito, H.; Kobayashi, T. *J. Cryst. Growth* **1996**, *158*, 437.
(22) Mokkapati, S.; Lever, P.; Tan, H. H.; Jagadish, C.; McBean, K. E.; Phillips, M. R. *Appl. Phys. Lett.* **2005**, *86*, 113102.
(23) Jensen, L. E.; Björk, M. T.; Jeppesen, S.; Persson, A. I.; Ohlsson, B. J.; Samuelson, L. *Nano Lett.* **2004**, *4*, 1961.

NL052189O